Dynamic Flying Height Adjustment in Hard Disk Drives Through Feedforward Control

Uwe Boettcher[1], Hui Li[2], Raymond A. de Callafon[1], and Frank E. Talke[1], *Fellow, IEEE*

[1]Department of Mechanical and Aerospace Engineering, Center for Magnetic Recording Research, University of California, San Diego, La Jolla, CA 92093-0401 USA

[2]Storage Mechanics Laboratory, Hitachi Asia Ltd., Singapore 049318, Singapore

A dynamic model of the resistance heater element in a thermal flying height control (TFC) slider of a hard disk drive is identified and used for dynamic flying height control. Experimental data obtained on a spin stand and a generalized realization algorithm are used for identification of a discrete-time dynamic model of the thermal actuator. The flying height change is measured in two different ways: using servo burst information written onto the disk surface and using information written in the data sectors only. The resistance change of the thermal actuator based on the input power level is measured. Based on the identified discrete-time model of the heater and using convex optimization techniques, a computational scheme is proposed to obtain optimized feedforward input profiles to the heater element that minimize repeatable flying height variations and enable low flying heights.

***Index Terms*—Actuators, feedforward systems, magnetic disk recording, resistance heating.**

I. Introduction

THE storage density has increased over eight orders of magnitude [1] since the IBM RAMAC was introduced in 1956. Two of the key technologies in achieving higher storage density are the reduction of the clearance between the read/write element and the recording medium and the minimization of flying height variations to maintain low bit error rates [2]. The flying height has decreased from initially about 20 μm [3] to a few nanometers in today's hard disk drives. The idea of actively controlling the flying height was introduced as early as 1990 [4]. The first design proposed in 1990 was based on a piezo element that allowed an adjustment of the read/write head relative to the disk surface. This technique was found to be difficult to implement at a cost-efficient mass production level. A different approach using thin-film microheaters for flying height control was first introduced by Mächtle *et al.* [5]. The use of a resistance heater element is now implemented in almost all current disk drives. This technique became necessary at low flying heights for various reasons. First, the write head causes thermal deformation of the air bearing surface towards the disk during the write process. This causes a different flying height during writing and reading, respectively, which is not desirable. To mitigate this effect and achieve the same flying height during reading and writing, heads were introduced featuring a resistance heater element that is positioned in close proximity to the read/write element. Fig. 1 shows a side view of the slider and the disk for this case. As can be seen from Fig. 1, the read/write element and the resistance heater are positioned at the trailing edge of the slider. Activating the resistance heater, one can reduce the head-disk clearance by Δd. Hence, the write current induced pole tip protrusion can be compensated by activating the resistance heater during reading. The second reason for the implementation of microheaters is that tolerances during manufacturing of the head can be relaxed and flying height changes due to changes in environmental conditions during operation can be compensated.

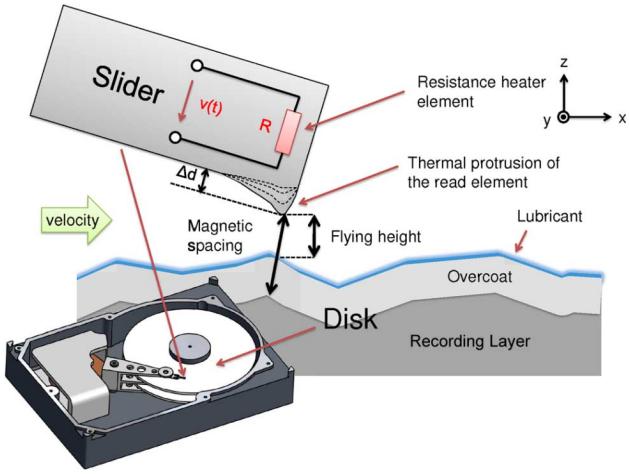

Fig. 1. Hard disk drive and side view of trailing edge of the slider with resistance heater element for thermal flying height control.

Thermal flying height control (TFC) is being applied in current disk drives in a "static sense", i.e., the power level applied to the heater is independent of the circumferential position of the slider over the disk. It is adjusted only depending on radial position, writing or reading operation and environmental conditions. However, the flying height in a disk drive varies in a dynamic manner [6]. Limited results are available on dynamically adjusting the TFC power to minimize flying height variations that occur along the circumference. One approach for dynamic flying height control has been shown by Shiramatsu *et al.* [7] who used a feedforward methodology without giving details on the control law that they used. An adaptive regulator scheme was proposed and simulated by Wu *et al.* [8] and experimental results using a piezo-electric actuator were recently given [9]. In the present paper, a different method of flying height control based on convex optimization is presented to solve the flying height variation minimization problem. Efficient solvers for those type of problems have been developed recently, which make real-time or nearly real-time applications

Manuscript received December 11, 2010; revised March 11, 2011; accepted March 23, 2011. Date of current version June 24, 2011. Corresponding author: U. Boettcher (e-mail: uwe@ucsd.edu).

Color versions of one or more of the figures in this paper are available online at http://ieeexplore.ieee.org.

Digital Object Identifier 10.1109/TMAG.2011.2136328

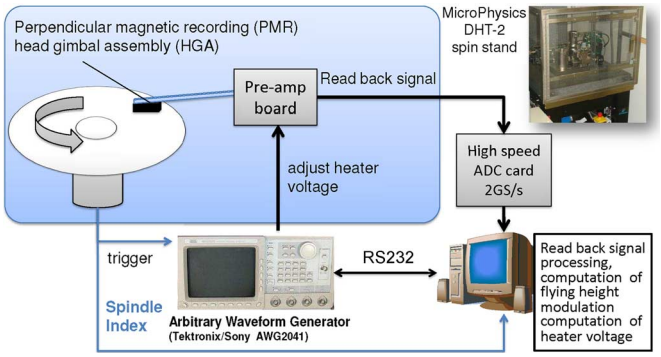

Fig. 2. Schematic of experimental spin stand setup.

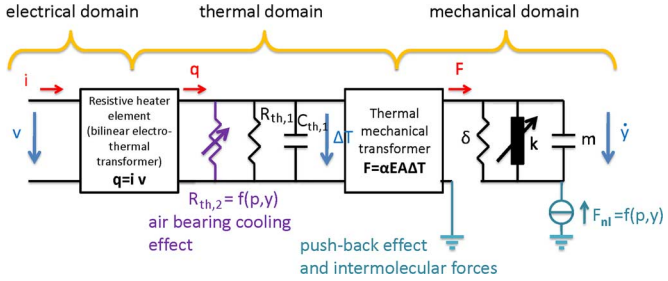

Fig. 3. Simplified network model of the resistance heater element including nonlinear effects such as air-bearing cooling effect and push-back effect.

feasible as shown in [10]. Hence, the optimal power profile to the heater element can be computed that minimizes repeatable circumferential variations of flying height. It should be noted that the computational effort of our approach is much larger compared to look-up tables that are precomputed during manufacturing calibration. However, this study indicates how optimal profiles can be obtained and stored in look-up tables. In addition, considering the increasing complexity and computational power in micro-controllers, one could utilize this additional degree of freedom to be able to adapt to changes in operational and/or environmental conditions.

The problem of dynamically adjusting the flying height can be divided into three main steps.

1) Measurement of flying height variation.
2) Data based estimation of dynamic heater response.
3) Computation of optimal input profile to the heater based on estimated model.

The first task will not be addressed in detail here, but steps 2 and 3 will be discussed in detail in the following sections.

II. Experimental Setup

Flying height data were obtained on a Disk-Head Tester (Microphysics spin stand model DHT-2) as shown in the schematic in Fig. 2. The measurements were performed at a radius of 28 mm, a skew angle of 1.3 degrees and a rotational speed of 7200 rpm. The relative magnetic spacing (which is assumed to correspond to the relative flying height) was computed in two different ways. First, the read back signal from the servo sectors on the disk was used in conjunction with the modified Wallace spacing loss formula. In this approach, we considered the A and B bursts of a conventional amplitude based servo pattern and computed the flying height change Δz from [11]

$$\Delta z = \frac{\lambda_1}{16\pi}\left(\ln(\Phi_{A1}+\Phi_{B1}) - 3\ln(\Phi_{A3}+\Phi_{B3})\right) \quad (1)$$

where $\Phi_{A,Bi}$ is the amplitude of the i^{th} harmonic of the A and B burst, respectively, and λ_1 is the wavelength of the first harmonic. A 16 T pattern consisting of 8 perpendicularly oriented "up" bits followed by 8 perpendicularly oriented "down" bits was employed as the servo pattern at a write frequency of 900 MHz. For this pattern, the first harmonic frequency occurs at 56.25 MHz. The second method used the conventional triple harmonics method [12], [13] to measure the flying height change based on data written in the servo sectors. The approach resulted in a higher sampling rate compared to the servo sector measurements. For this method, the flying height change was computed as

$$\Delta z = \frac{\lambda_1}{4\pi}\left(\ln(\Phi_1) - \ln(\Phi_3)\right) \quad (2)$$

where Φ_1 and Φ_3 represent the first and third harmonic of the read back signal, respectively. The read back signals in the servo and data sectors were sampled at 2 GHz. A total number of 128 servo sectors corresponds to a sampling frequency of the flying height modulation of 15.36 kHz for the first method. The resolution of the data sector based method contains a trade-off between time-domain and frequency-domain accuracy. A number of 20 flying height measurements per data sector was chosen yielding an effective sampling rate of 380 kHz which is significantly higher than the sampling rate of the servo sector based method. A waveform generator was used to apply the power profile to the heater. The spindle index signal was used as a trigger.

III. Dynamic Modeling of the Heater Response

A. Modeling Based on Physical Principles

To model the flying height variation induced by the thermal actuator based on physical principles is complicated and contains several effects that have been reported in the literature; a short overview is given in the following. As can be seen from Fig. 3, the system ranges over three physical domains, i.e., electrical, thermal and mechanical. The power applied to the heater causes a resistive heating (Joule heating) of the heater element and its surrounding materials. This, in turn, causes a thermal deformation of the air bearing surface which positions the read/write element closer to the disk as indicated in Fig. 1. There are several effects that counteract the thermally induced flying height reduction.

1) Electrical domain: The resistance of the heater element changes as the temperature increases which changes the Joule heating effect (Fig. 5).
2) Thermal domain: It was found in [14] that the main heat exchange between the head and the disk is through heat conduction. As the distance between the thermal protrusion and the disk is reduced, the conductive heat exchange between the head and disk is affected by the local air bearing pressure and the decrease in the mean free path of the air in the gap between thermal protrusion and disk. This is known as the air bearing cooling effect [15], [16].
3) Mechanical domain: A local increase in air bearing pressure causes a so-called push-back effect which is indicated in

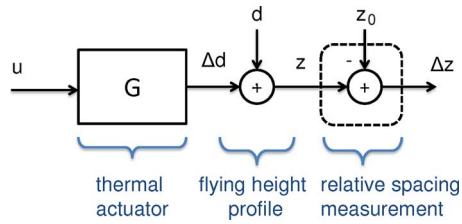

Fig. 4. Schematic of thermal actuator and flying height sensor.

Fig. 3 by the nonlinear force F_{nl} acting on the output. Furthermore, in the close-contact regime, intermolecular and electrostatic forces will play a role as has been shown in [17].

B. Data-Based Modeling Approach

A data-based (black-box) modeling approach seems more feasible than a model derivation based on physical principles considering the presence of numerous parameter uncertainties. A schematic of the actuator and measurement system is shown in Fig. 4. Here, u represents the input power applied to the thermal actuator G. The flying height variation d is considered an unknown disturbance to be rejected by the thermal actuator. In the experimental setup described in Section II, the absolute spacing z is not measurable. However, the spacing variation relative to an initially unknown flying height z_0 can be measured where

$$\Delta z = z - z_0. \tag{3}$$

The contribution of the actuator to the flying height change can be estimated by performing two experiments: one without a dynamic input signal as a reference measurement and a second experiment using an input signal which is "persistently exciting". A good choice is a step input signal. The step data can then be used to identify a discrete-time model of the actuator using the generalized realization algorithm as presented in [18], [19]. The algorithm will be briefly reviewed below. It computes the state space matrices $\mathbf{A}$, $\mathbf{B}$ and $\mathbf{C}$ of a discrete-time model of the thermal actuator, illustrated in Fig. 4. The input/output relationship of the heater system shown in Fig. 4 can be written as

$$\mathbf{\Delta D} = \mathbf{HU} + \mathbf{E} \tag{4}$$

where $\mathbf{\Delta D}$ is a Hankel matrix of the output signals defined in (9), $\mathbf{U}$ is the input matrix (upper triangular matrix with only ones) and $\mathbf{H}$ is a Hankel matrix that contains the Markov parameters $g(k)$ that are defined by

$$g(k) = \begin{cases} \mathbf{D} & \text{for } k = 0 \\ \mathbf{CA^{k-1}B} & \text{for } k \geq 1 \end{cases}. \tag{5}$$

This forms the matrix

$$\mathbf{H} = \mathbf{\Gamma\Omega}. \tag{6}$$

In (6), $\mathbf{\Gamma}$ and $\mathbf{\Omega}$ are the observability and controllability matrix, respectively, defined by

$$\mathbf{\Gamma} = \begin{bmatrix} \mathbf{C} \\ \mathbf{CA} \\ \vdots \\ \mathbf{CA^{k-1}} \end{bmatrix}, \ \mathbf{\Omega} = \begin{bmatrix} \mathbf{B} & \mathbf{AB} & \cdots & \mathbf{A^{k-1}B} \end{bmatrix}. \tag{7}$$

The matrix $\mathbf{E}$ in (4) contains the effect of past input signals multiplied by the Markov parameters of the system. For a step-function as an input, $\mathbf{E}$ is a row-wise listing of past output signals [20] and yields

$$\mathbf{E} = \begin{bmatrix} \Delta d(0) & \cdots & \Delta d(0) \\ \vdots & \vdots & \vdots \\ \Delta d(N-1) & \cdots & \Delta d(N-1) \end{bmatrix}. \tag{8}$$

A realization is performed based on the weighted Hankel matrix $\mathbf{R} = \mathbf{\Delta D} - \mathbf{E}$, allowing the use of step function input signals instead of impulse response measurements.

The measured step data are stored in a $N \times N$ Hankel matrix

$$\mathbf{\Delta D} = \begin{bmatrix} \Delta d(1) & \Delta d(2) & \cdots & \Delta d(N) \\ \Delta d(2) & \Delta d(3) & \cdots & \Delta d(N+1) \\ \vdots & \vdots & \vdots & \vdots \\ \Delta d(N) & \Delta d(N+1) & \cdots & \Delta d(2N-1) \end{bmatrix} \tag{9}$$

where N denotes the number of data points for each measurement. The vector Δd denotes the measured step response. The weighted Hankel matrix $\mathbf{R}$ is defined as

$$\mathbf{R} = \mathbf{\Delta D} - \mathbf{E} = \mathbf{HU} \tag{10}$$

and has the same rank as $\mathbf{H}$. The matrix $\mathbf{R}$ is decomposed into an $\mathrm{N} \times \mathrm{n}$ matrix $\mathbf{R_1}$ and an $\mathrm{n} \times \mathrm{N}$ matrix $\mathbf{R_2}$, by using singular value decomposition. This decomposition allows choosing the rank n of the matrix, and, thus, the order of the estimated model. The singular value decomposition applied to $\mathbf{R}$ yields

$$\mathbf{R} = \mathbf{U\Sigma V}^{\mathrm{T}} = [U_{\mathrm{n}}\, U_{\mathrm{s}}] \begin{bmatrix} \Sigma_{\mathrm{n}} & 0 \\ 0 & \Sigma_{\mathrm{s}} \end{bmatrix} \begin{bmatrix} V_{\mathrm{n}}^{\mathrm{T}} \\ V_{\mathrm{s}}^{\mathrm{T}} \end{bmatrix} \tag{11}$$

where $\mathbf{V}$ and $\mathbf{U}$ are unitary matrices, and $\mathbf{\Sigma}$ is a diagonal matrix that contains the singular values of the original matrix. In (11), Σ_n stores the n largest singular values and Σ_s contains the remaining smaller part. The unitary matrices are divided in a similar fashion into $U_{\mathrm{n,s}}$ and $V_{\mathrm{n,s}}$, respectively. Using the singular value decomposition $\mathbf{R}$ is reduced to a rank n matrix

$$\mathbf{R}_{\mathrm{n}} = \mathbf{R_1 R_2} \tag{12}$$

where

$$\mathbf{R_1} = \mathbf{U}_{\mathrm{n}} \mathbf{\Sigma}_{\mathrm{n}}^{\mathbf{1/2}}, \quad \mathbf{R_2} = \mathbf{\Sigma}_{\mathrm{n}}^{\mathbf{1/2}} \mathbf{V}_{\mathrm{n}}^{\mathrm{T}}. \tag{13}$$

With (7) we have $\mathbf{R_1} = \mathbf{\Gamma}$ and $\mathbf{R_2} = \mathbf{\Omega U}$ where $\mathbf{U}$ has full rank. A shifted version of $\mathbf{R}$ is defined by

$$\bar{\mathbf{R}} = \bar{\mathbf{\Delta D}} - \bar{\mathbf{E}} \tag{14}$$

where each element is shifted one sample forward in time. Hence, $\bar{\mathbf{\Delta D}}$ becomes

$$\bar{\mathbf{\Delta D}} = \begin{bmatrix} \Delta d(2) & \Delta d(3) & \cdots & \Delta d(N+1) \\ \Delta d(3) & \Delta d(4) & \cdots & \Delta d(N+2) \\ \vdots & \vdots & \vdots & \vdots \\ \Delta d(N+1) & \Delta d(N+2) & \cdots & \Delta d(2N) \end{bmatrix} \tag{15}$$

and $\bar{\mathbf{E}}$ is defined in a similar fashion.

From (5) and (7) it can be shown that

$$\bar{\mathbf{R}} = \mathbf{\Gamma A \Omega U} = \mathbf{R_1 A R_2} \tag{16}$$

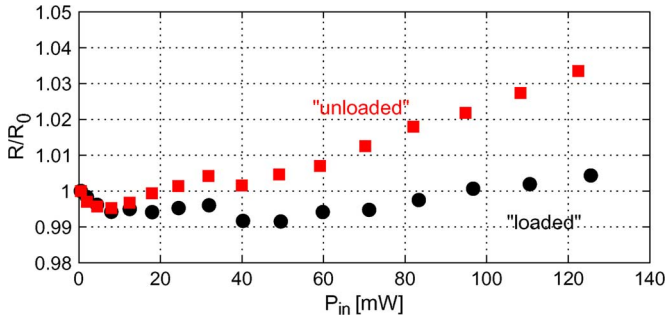

Fig. 5. Dependence of the heater resistance on the input power level for a loaded and unloaded head.

$\mathbf{R_1}$, $\mathbf{R_2}$ and $\bar{\mathbf{R}}$ in (16) are computed in previous steps. Hence, the state matrix $\mathbf{A}$ can be estimated by

$$\mathbf{A} = \mathbf{R_1^*}\bar{\mathbf{R}}\mathbf{R_2^*} \tag{17}$$

where

$$\mathbf{R_1^*} = \mathbf{\Sigma_n^{-1/2}}\mathbf{U_n^T}, \quad \mathbf{R_2^*} = \mathbf{V_n}\mathbf{\Sigma_n^{-1/2}} \tag{18}$$

denote the left and right inverse of (13), respectively.

From (7) it can be observed that the input matrix $\mathbf{B}$ is the first column of $\mathbf{R_2}$ and that the first row of $\mathbf{R_1}$ forms the output matrix $\mathbf{C}$.

The feed-through term $\mathbf{D}$ contains only the first data point of the output signal after an input step, i.e., $\mathbf{D} = \Delta d(0)$. The D matrix could also be estimated by solving a least-square problem but in the present case it can also be set to zero as one sample time-delay can be assumed for the thermal actuator.

C. Modeling Algorithm Applied to Experimental Data

The described modeling procedure was applied to the heater element in the TFC slider. Voltage steps v were applied to the heater element and the input power P was computed using $P = \mathrm{v}^2/R$ assuming a fixed value for the heater resistance R. This assumption is reasonable since it was found experimentally that the resistance of the heater element is not a strong function of the applied voltage. Fig. 5 shows the change in resistance based on different input power levels for the case that the head is flying on the disk (loaded) and the case that the head is stationary away from the disk without an air bearing present (unloaded). The unloaded case shows a much higher increase in heater resistance compared to the loaded case which is likely related to the heat transfer from the head to the disk [15]. The dynamic response to a 2 V-step input for three different bias voltages (3.5, 4.0 and 4.5 V) is measured. The results are shown in Fig. 6 and Fig. 7, respectively. In Fig. 6 the flying height change is determined using the servo sector approach [11] and in Fig. 7 the flying height change is estimated based on data sector measurements. The simulated response using estimated 2nd order models can be seen in Figs. 6 and 7 as the solid lines. We observe that the estimated models are in excellent agreement with the measurements. By estimating only a first order model of the heater response, one would observe a significant modeling error. It is also noted that the responses are in qualitative agreement with recent numerical studies [21]. The Bode plots of the resulting 2nd order continuous-time models assuming zero-order-hold for the 380 kHz sampling frequency case are shown in Fig. 8. One can observe the presence of two time constants in the Bode plot. The

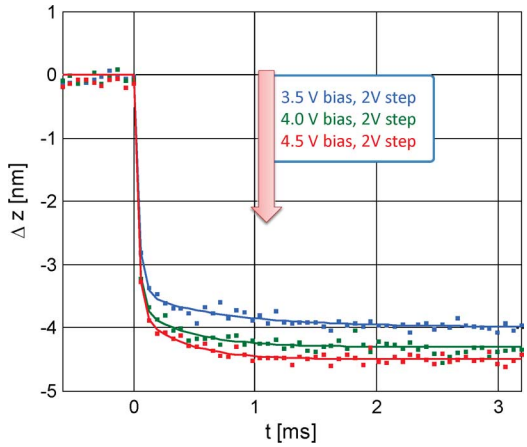

Fig. 6. Dynamic response of the relative flying height to voltage step inputs measured using the servo sectors [11] at a sampling rate of 15.36 kHz and estimated 2nd order model (solid lines).

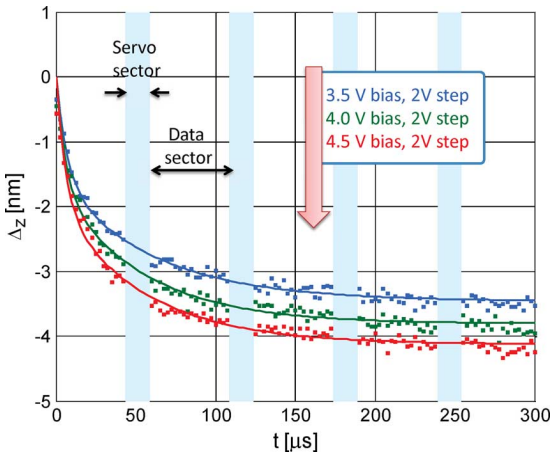

Fig. 7. Dynamic response of the relative flying height to voltage step inputs measured using the data sectors at an effective sampling rate of 380 kHz and estimated 2nd order models (solid lines).

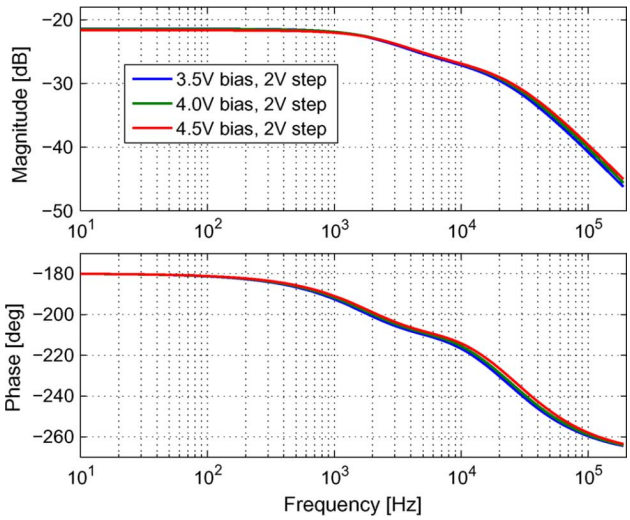

Fig. 8. Bode response of zero-order-hold equivalent continuous-time models estimated from discrete-time models at 380 kHz.

TABLE I
PARAMETER OF 2ND ORDER DISCRETE-TIME MODELS

Bias	sampling rate	a	b	c	d
3.5 V	15.35 kHz	-0.06847	0.06162	-1.108	0.1789
4.0 V	15.35 kHz	-0.07005	0.05851	-1.005	0.1277
4.5 V	15.35 kHz	-0.06536	0.05299	-0.9887	0.1266
3.5 V	380 kHz	-0.01333	0.01237	-1.674	0.6858
4.0 V	380 kHz	-0.01418	0.01311	-1.657	0.6699
4.5 V	380 kHz	-0.01499	0.01378	-1.631	06454

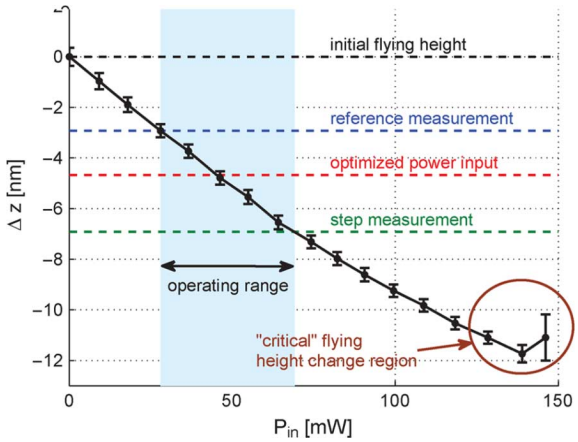

Fig. 9. Touch down experiment showing the mean value of the flying height change over the circumference for the averaged (20 averages) flying height measurements and the variance.

estimated second order models can be parameterized in the discrete-time transfer function form

$$G(z) = \frac{\mathrm{a}z + \mathrm{b}}{z^2 + \mathrm{c}z + \mathrm{d}} \tag{19}$$

where the model parameters a, b, c and d are given in Table I for the 6 identified models.

In the remainder of this paper we consider only the flying height change measurements based on the servo sector approach since this is the more practical approach in an HDD application.

The step experiments were performed approximately 3 nm below the initial flying height (without power input to the heater) after applying a bias voltage. Fig. 9 shows the change in average flying height Δz versus heater power. We observe that the flying height decreases almost linearly as the heater power increases. In the close-contact regime, at the far right of the figure, the flying height change stops to decrease and the variance of the averaged signal increases. At this "critical" flying height, slider vibrations at the air bearing frequency near 300 kHz can be observed in the read back signal (Fig. 10). It should be noted that the dynamic and static behavior of the thermal actuator is inherently nonlinear in extremely close proximity to the disk and highly dependent on the absolute spacing of the head over the disk as indicated in Section III-A. Therefore, for our dynamic flying height control studies, we restrict our attention to the range depicted as "operating range" in Fig. 9. The initial flying height (0 mW heater input) in our experiment is around 11–12 nm and the operating range is 3 to 7 nm below the initial flying height.

In order to compute the optimal feedforward profile in the given operating range (Fig. 9), we estimate a dynamic model

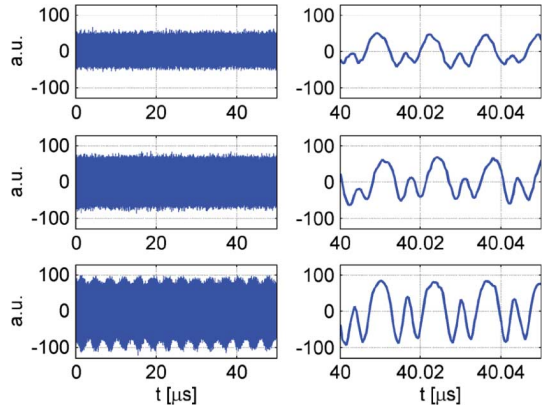

Fig. 10. Measured read back signal of the data sector for three different flying heights: a) initial, b) −8 nm, c) −12 nm.

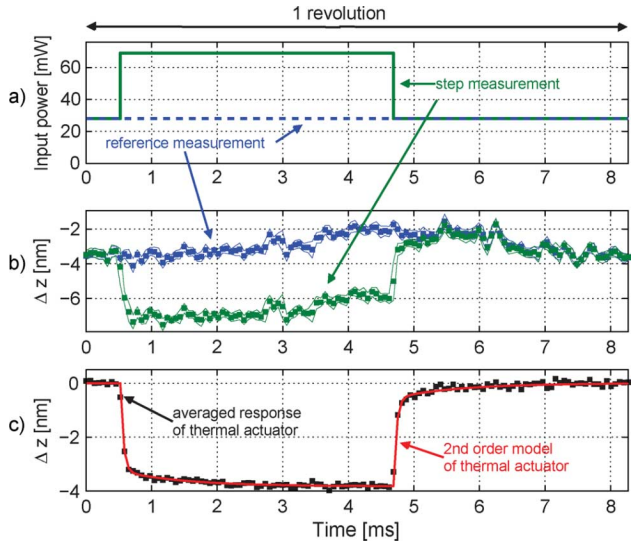

Fig. 11. Averaged spin stand measurement (20 averages). a) Power input: reference and step power. b) Corresponding measured flying height variation (averaged values and standard derivation). c) Identified 2nd order model and relative averaged spacing measurement.

of the thermal actuator within that range. The results are shown in Fig. 11 where Fig. 11(a)) shows the reference input power and the step input power. The flying height change Δz (response) can be seen in Fig. 11(b)). The squares in Fig. 11(b)) represent the averaged values (20 averages) obtained at each of the 128 servo sectors and the lines in the neighborhood of the squares represent the standard deviation. The flying height change due to the thermal actuator is the difference between the two flying height change measurements in Fig. 11(b)) and is shown in Fig. 11(c)). The simulated flying height change of the estimated 2nd order model is plotted in Fig. 11(c)) as well.

For maximum read back performance, the operating flying height range of the read/write element should be as close as possible to the disk. The flying height in an HDD needs to be reduced to approximately 1 nm as the storage density approaches 1 $\mathrm{Tb/in^2}$ [22]. As seen in Fig. 9, this introduces nonlinear effects for the head gimbal assembly used in this study. These nonlinear effects are beyond the scope of this paper but will be of interest for future work. Here, we restrict ourselves to show how repeatable flying height variations can be minimized for the operational range depicted in Fig. 9.

IV. Computing Optimal Power Profile

A. Development of the Optimization Algorithm

If the flying height change generated by the thermal actuator matches the inverse of the flying height modulation, a constant flying height is obtained. The computation of the power profile based on the inverse of the flying height modulation is not trivial as the inverse of the actuator model is not necessarily stable and, in addition, noncausal. Furthermore, the fact that the control energy is limited should be taken into account. The problem at hand can be formulated as a convex optimization problem where the flying height modulation is minimized in a 2-norm sense. The direct computation of a feedforward profile makes the design of a feedforward filter redundant.

The second order model of the identified heater actuator is written in state space form as

$$\begin{aligned} x(k+1) &= \mathbf{A}x(k) + \mathbf{B}u(k) \\ \Delta d(k) &= \mathbf{C}x(k) \end{aligned} \tag{20}$$

where $\mathbf{A}$, $\mathbf{B}$ and $\mathbf{C}$ follow from the identification procedure described in Section III.

Following [23], we can recursively re-write the actuator output Δd as

$$\begin{aligned} \Delta d(0) &= Cx(0) \\ \Delta d(1) &= CAx(0) + CBu(0) \\ \Delta d(2) &= CA^2x(0) + CABu(0) + CBu(1) \\ &\vdots \\ \Delta d(N-1) &= CA^{N-1}x(0) + \sum_{i=1}^{N-1} CA^{N-i}Bu(i-1) \end{aligned} \tag{21}$$

or in matrix form

$$\mathbf{\Delta d} = \mathbf{\Psi u} \tag{22}$$

where

$$\mathbf{\Psi} = \begin{bmatrix} 0 & 0 & 0 & \cdots & 0 \\ CB & 0 & 0 & \cdots & 0 \\ CAB & CB & 0 & \cdots & 0 \\ \vdots & \vdots & \vdots & \cdots & \vdots \\ CA^{N-2}B & CA^{N-3}B & & \cdots & 0 \\ CA^{N-1}B & CA^{N-2}B & & \cdots & CB \end{bmatrix}. \tag{23}$$

The initial value of the state $x(0)$ is set to zero. Based on this definition, the following optimization problem can be stated:

$$\begin{aligned} \min_{\mathbf{u}} \; & \|\mathbf{\Psi u} + \mathbf{d} - \inf(\mathbf{d}) - \Delta z_0\|_2 \\ \text{subject to } & \mathbf{u} \le \mathbf{u}_{\max} \\ & \mathbf{u} \ge \mathbf{u}_{\min}. \end{aligned} \tag{24}$$

The motivation to pose the optimization problem as shown in (24) is as follows. A flying height lower than the infimum (in this case minimum) of the flying height modulation d is desired since no negative power can be applied to the heater. An additional spacing parameter $\Delta z_0 > 0$ is required to reduce the flying height. Linear constraints on the input power u are imposed through energy and design limitations on the thermal actuator reflected by $\mathbf{u_{max}}$ and $\mathbf{u_{min}}$. In a hard disk drive application, Δz_0 could be increased until the minimum stable flying height is reached. Minimizing the Euclidean norm as in (24) is equivalent to minimizing the Euclidean norm squared [24]. Thus, the problem can be reformulated as a quadratic programming problem or a semidefinite programming problem. For no or very loose constraints on the actuator signal, the problem can be reduced to a conventional nonconstrained least-squares optimization problem which may be sufficient in an actual hard disk drive.

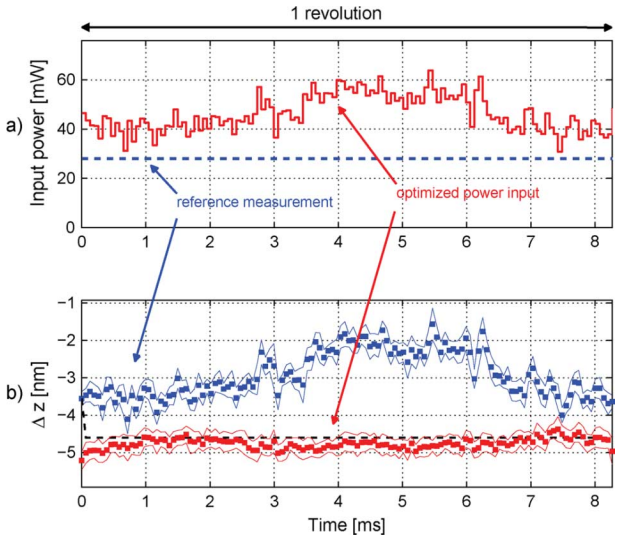

Fig. 12. Averaged spin stand measurement (20 averages): a) power input: reference signal, optimized signal. b) corresponding measured flying height variation (averaged values and standard derivation).

B. Optimization Algorithm Applied to Experimental Setup

The model of the heater element estimated in Section III and (24) was used to compute an optimized power input signal. The CVX software package [25] was used to solve the optimization problem. Δz_0 was chosen to be 0.5 nm because a bias voltage was already applied to the heater. For our experimental conditions, this yields an approximate absolute flying height of 7–8 nm. The measurements are shown in Fig. 12. We characterize the flying height variation by the difference between maximum and minimum value due to repeatable (averaged) variations (dots in Fig. 12(b)) and the variance due to nonperiodic variations (solid lines in Fig. 12(b)). It is clear from Fig. 12 that our feedforward compensation targets the repeatable variations by minimizing the difference between maximum and minimum averaged value, creating an almost flat averaged profile of flying height variations. For comparison purposes, the dashed line in Fig. 12(b) indicates the prediction of the feedforward compensation based on our linear model. The good agreement between experiments and simulation indicates a) validation of our model and b) successful computation of the optimized feedforward profile. The variance due to nonperiodic variations remains almost the same.

The measured optimized flying height profile depicted in Fig. 12(b) shows much smaller flying height variations than the reference measurement (nonoptimized). We note, in particular, that the difference between maximum and minimum value is reduced from 2.54 nm to 0.84 nm. These results show that the

technique used is very promising and potentially of great use in future disk drives.

V. Conclusion

A discrete-time dynamic model of a thermal flying height actuator in a hard disk drive was identified using step experiments and a generalized realization algorithm. The flying height change measurements used in this study were based on two different measurement techniques with sampling rates of 15.36 kHz and 380 kHz, respectively. It was found that the heater response can be modeled sufficiently well with a second order model that captures both a fast and a slow time constant observed in the heater step response. The resistance change of the thermal actuator was measured as a function of the input power and found to be within a few percent of the case of a flying slider (loaded). It was shown that convex optimization techniques can be used to significantly minimize circumferential flying height variations in a disk drive based on the identified heater actuator model. Spin stand experiments showed that the maximum-minimum value difference of the averaged flying height variations was reduced to about one third compared to the initial reference measurement where no power optimization was performed. Since the proposed method is a true feedforward technique it can only compensate repeatable flying height variations. Both the simulated step response and the simulated response to the optimized input signal are in good agreement with experimentally obtained results. Small variations can be explained with modeling and measurement errors. The presented algorithms on heater dynamics modeling and input power optimization are not computationally expensive and could be implemented in the firmware of the hard disk drive. This might enable an increase in durability and reliability of the drive while decreasing flying height and bit error rate. The identified linear model of the heater becomes invalid in the close-contact regime due to nonlinearities. Future work should involve nonlinear modeling approaches and adaptive feedforward approaches to minimize the flying height while maintaining a minimum in flying height variations. A final point is related to the response time of the thermal actuator. Even though thermal equilibrium was only reached after a few milliseconds, the second (fast) time constant of the thermal actuator enables flying height adjustment up to several kHz.

Acknowledgment

The authors would like to thank T. Crittenden and C. Lacey of Microphysics, Inc., G. Kimball of Texas Instruments and J. Contreras of Hitachi Global Storage Technologies, Ltd. for their help with the experimental setup.

References

[1] Y.-T. Hsia, "The ever shrinking hard disk drive and its components: What are the challenges?," in *Int. Symp. Micro-NanoMechatronics and Human Science*, Nov. 2006, pp. 1–2.

[2] Y. Tang, S.-Y. Hong, N.-Y. Kim, and X. Che, "Overview of fly height control applications in perpendicular magnetic recording," *IEEE Trans. Magn.*, vol. 43, no. 2, pp. 709–714, Feb. 2007.

[3] J. M. Harker, D. W. Brede, R. E. Pattison, G. R. Santana, and L. G. Taft, "A quarter century of disk file innovation," *IBM J. Res. Develop.*, vol. 25, no. 5, pp. 677–690, Sep. 1981.

[4] C. Yeack-Scranton, V. Khanna, K. Etzold, and A. Praino, "An active slider for practical contact recording," *IEEE Trans. Magn.*, vol. 26, no. 5, pp. 2478–2483, Sep. 1990.

[5] P. Machtle, R. Berger, A. Dietzel, M. Despont, W. Haberle, R. Stutz, G. Binnig, and P. Vettiger, "Integrated microheaters for in-situ flying-height control of sliders used in hard-disk drives," in *The 14th IEEE International Conference on Micro Electro Mechanical Systems (MEMS)*, 2001, pp. 196–199.

[6] J. Xu, Y. Shimizu, and L. Su, "Drive level measurement of flying height modulation and control of slider disk contact," *Tribol. Lett.*, vol. 24, pp. 159–162, 2006.

[7] T. Shiramatsu, T. Atsumi, M. Kurita, Y. Shimizu, and H. Tanaka, "Dynamically controlled thermal flying-height control slider," *IEEE Trans. Magn.*, vol. 44, no. 11, pp. 3695–3697, Nov. 2008.

[8] Z. Wu and F. Amara, "Adaptive regulation of the flying height in hard disk drives," in *Proc. IEEE Conf. Control Applications*, Toronto, Canada, Aug. 28–31, 2005, pp. 1146–1151.

[9] Z. Wu and F. Amara, "Adaptive regulation in switched bimodal systems: An experimental evaluation," *IEEE Trans. Control Syst. Technol.*, vol. 18, no. 4, pp. 885–895, Jul. 2010.

[10] J. Mattingley and S. Boyd, "Real-time convex optimization in signal processing," *IEEE Signal Process. Mag.*, vol. 27, no. 3, pp. 50–61, May 2010.

[11] U. Boettcher, C. Lacey, H. Li, K. Amemiya, R. de Callafon, and F. Talke, "Servo signal processing for flying height control in hard disk drives," *Microsyst. Technol.* pp. 1–8, 2011, 10.1007/s00542-010-1193-7 [Online]. Available: http://dx.doi.org/10.1007/s00542-010-1193-7

[12] Z.-M. Yuan, B. Liu, W. Zhang, and S.-B. Hu, "Engineering study of triple-harmonic method for in situ characterization of head-disk spacing," *J. Magn. Magn. Mater.*, vol. 239, no. 1-3, pp. 367–370, 2002.

[13] B. Liu and Z. Yuan, "Tribo-magnetics and nanometer spaced head-disk systems," in *Asia-Pacific Magnetic Recording Conf. (APMRC 2000)*, Dec. 2000, pp. TB5/1–TB5/2.

[14] D. Chen and D. Bogy, "Simulation of static flying attitudes with different heat transfer models for a flying-height control slider with thermal protrusion," *Tribol. Lett.*, vol. 40, pp. 31–39, 2010.

[15] J.-Y. Juang and D. B. Bogy, "Air-bearing effects on actuated thermal pole-tip protrusion for hard disk drives," *J. Tribol.*, vol. 129, no. 3, pp. 570–578, 2007.

[16] J. Fritzsche, H. Li, H. Zheng, K. Amemiya, and F. E. Talke, "The effect of air bearing contour design on thermal pole-tip protrusion," in *ASME Information Storage and Processing Systems Conf.*, Santa Clara, CA, 2010.

[17] V. Gupta and D. Bogy, "Dynamics of sub-5-nm air-bearing sliders in the presence of electrostatic and intermolecular forces at the head-disk interface," *IEEE Trans. Magn.*, vol. 41, no. 2, pp. 610–615, Feb. 2005.

[18] R. A. de Callafon, B. Moaveni, J. P. Conte, X. He, and E. Udd, "General realization algorithm for modal identification of linear dynamic systems," *J. Eng. Mech.*, vol. 134, no. 9, pp. 712–722, 2008.

[19] U. Boettcher, B. Raeymaekers, R. de Callafon, and F. Talke, "Dynamic modeling and control of a piezo-electric dual-stage tape servo actuator," *IEEE Trans. Magn.*, vol. 45, no. 7, pp. 3017–3024, 2009.

[20] R. de Callafon, "Estimating parameters in a lumped parameter system with first principle modeling and dynamic experiments," in *Proc. 13th IFAC Symposium on System Identification*, Rotterdam, The Netherlands, 2003, pp. 1613–1618.

[21] H. Li, H. Zheng, J. Fritzsche, K. Amemiya, and F. Talke, "Simulation of flying height and response time of thermal flying height control sliders with thermal insulators," *IEEE Trans. Magn.*, vol. 46, no. 6, pp. 1292–1294, 2010.

[22] S. Ookubo, T. Shiramatsu, M. Kurita, H. Kohira, and Y. Takeuchi, "Investigation of mechanical clearance change with thermal flying-height control slider at high altitude," *J. Adv. Mech. Des., Syst., Manuf.*, vol. 4, no. 1, pp. 32–41, 2010.

[23] G. Goodwin, M. Seron, and J. de Dona, *Constrained Control and Estimation: An Optimization Approach*. London, U.K.: Springer Verlag, 2005.

[24] S. Boyd and L. Vandenberghe, *Convex Optimization*. New York: Cambridge University Press, 2004.

[25] M. Grant and S. Boyd, "CVX: Matlab Software for Disciplined Convex Programming," ver. 1.21, Sep. 2010 [Online]. Available: http://cvxr.com/cvx